Thermodynamic equilibria-based modelling of reactive chloride transport in blended cementitious materials

Rachid Cherif, Ameur El Amine Hamami, Abdelkarim Aït-Mokhtar, Walter Bosschaerts

Thermodynamic equilibria-based modelling of reactive chloride transport in blended cementitious materials

Rachid CHERIF[a,*], Ameur El Amine HAMAMI[a], Abdelkarim AÏT-MOKHTAR[a], Walter BOSSCHAERTS[b]

[a]University of La Rochelle-CNRS, LaSIE UMR 7356, Avenue Michel Crépeau, 17042 La Rochelle Cedex 1, France
[b]Royal Military Academy, Department of Mechanics, Rue Hobbema 8, 1000 Brussels, Belgium

*** Corresponding author:**
e-mail address: rachid.cherif@univ-lr.fr
Tel: +33 5.46.45.72.30.

Thermodynamic equilibria-based modelling of reactive chloride transport in blended cementitious materials

Abstract

A physico-chemical modelling of multispecies transport through cementitious materials is proposed considering thermodynamic equilibria, diffusion and migration. The model considers seven species profiles (Cl^-, Na^+, K^+, Ca^{2+}, SO_4^{2-}, $Al(OH)_4^-$ and OH^-) and the dissolution/precipitation rates during multispecies transport under an electrical field. The fluxes are calculated by the Nernst-Planck equation. Case studies were performed simulating the chloride migration test in the steady state and NT Build 492 test on cement pastes based on slag and/or Portland cement. In order to simulate real exposure to seawater, the migration tests were based on synthetic seawater in the upstream compartment and a synthetic pore solution in the downstream. Pore solution extractions and scanning electron microscopy were performed in order to provide input data and to monitor dissolution/precipitation reactions. The proposed modelling highlights a reduction of up to 10% of free chlorides in the material tested compared to the classic Nernst-Planck modelling.

***Keywords**:* transport modelling, durability, chlorides, dissolution/precipitation rates, scanning electron microscopy.

***Abbreviations**:* PNP, Poisson–Nernst–Planck; C-S-H, Calcium silicate hydrate; CH, Portlandite; AFm, monosulfoaluminates; AFt, Ettringite; FS, Friedel's salt; KS, Kugel's salt; K, Thermodynamic equilibrium constant; j, Flux [mol.m^{-2}.s^{-1}]; D, Diffusion coefficient [m^2.s^{-1}]; i, Ion i; C, Concentration [mol.m^{-3}]; $C_{i,b}$, Ion concentration bonded to the cement matrix; z, Valence; F, Faraday constant [C.mol^{-1}]; R, Perfect gas constant [J.mol^{-1}.K^{-1}]; T, Temperature [K]; Ψ, Electrical potential [V]; E, Electrical field [V.m^{-1}]; φ, Total porosity; τ, Tortuosity; a, Chloride isotherm constant; f, Formation factor; q, Mass exchange term [mol.m^{-3}.s^{-1}]; Ω_m Saturation ratio of the mineral m; χ, Kinetic constant [mol.m^{-2}.s^{-1}]; A, Reactive specific surface [m^2.kg^{-1}]; r, Rate of dissolution/precipitation; n, Stoichiometric number; m_s, Sample mass [kg], ρ_s, Sample density [kg.m^{-3}]; M_{H_2O}, Molecular weight of H_2O [kg.mol^{-1}]. CP, Cement paste with Portland cement; BFS75, Cement paste with 75% of Blast furnace slag; W/B, Water to binder ratio; E-SEM, Scanning electron microscopy in environmental mode; TGA, Thermogravimetric analysis.

1. Introduction

The European standard EN 206-1/CN and the different recommendations it gives have defined exposure classes and approaches to determine some parameters known as durability indicators [1]. One of these indicators is the chloride diffusion coefficient for reinforced concrete structures in marine areas. Chloride diffusion is governed, on the one hand, by a concentration gradient between seawater and the concrete pore solution and, on the other hand, by advection in partially saturated concrete (tidal areas or marine fogs), when heat and moisture transfers occur [2,3]. When chlorides reach a threshold concentration in the reinforced concrete, they generate the rebar depassivation and then the rebar corrosion [4–6]. It has been shown that chloride penetration through the concrete pores also generates a thermodynamic disequilibrium of the system hydrates-pore solution [7–10]. This leads to a modification of the microstructure and pore solution composition [11–14]. Indeed, chlorides interact with anhydrous C_3A and C_4AF and the other ions initially present in the pore solution or those resulting from hydrates dissolution [10,15–17]. These interactions produce novel solid phases in the pores such as $CaCl_2$, oxychlorides ($3CaO.CaCl_2.15H_2O$), Friedel's and Kugel's salts ($3CaO.Al_2O_3.CaCl_2.10H_2O$ and $Ca_4.Al_2(SO_4)_{0.5}.Cl(OH)_{12}.6H_2O$, respectively), etc. [13,16].

In order to estimate the concrete's resistance to the chloride penetration, Andrade [18] presented a reliable method for the calculation of the effective diffusion coefficient of chlorides. The approach was based on electrochemistry fundamentals using the Nernst-Planck and Nernst-Einstein equations. This single-species approach has been enhanced by Amiri et al. [19]. Later, several multispecies models of chloride transfer in cementitious materials were developed [20–27]. Jiang et al. [28] gave a methodology for predicting the chloride concentration profiles of concrete exposed to chlorides. The

modelling was based on the Poisson–Nernst–Planck (PNP) equation, considering the chemical activity, electrophoreses and the relaxation. Xia and Li [29] presented a numerical modelling of the ion transport in saturated cement pastes considering the interactions between the monovalent ions of the pore solution (electrostatic coupling). The modelling was based on PNP equations. The results show that the chloride profiles of the cement pastes significantly change with the pore solution composition (initial concentrations). They concluded that chloride transport depends on the pore solution composition and multispecies interactions. Fenaux et al. [30] proposed a model of chloride transport through saturated concrete which takes into account the usual monovalent ions (Cl^-, Na^+, K^+ *and* OH^-) and Ca^{2+} as a divalent ion of the pore solution; the sulfates were neglected. The modelling integrates the diffusion, migration and chemical activity. The latter was calculated using the Pitzer model. The results discussed the influence of the pore solution on the chloride penetration. Also, the consideration of the chemical activity slightly improves the prediction of the concentration profiles of the studied species.

More recently, chloride transport models including thermodynamic equilibria were developed [9,10,31–35]. Jensen et al. [9,31] proposed a multispecies modelling of reactive mass transport through saturated cementitious materials based on PNP equations, accounting for chemical equilibrium. Solid and/or solution reactions during chloride transfer and chemical equilibria were determined by the geochemical code PhreeqC®. The model was applied for simulating chloride profiles in saturated mortars exposed for 180 days to an NaCl solution and seawater. Yu and Zhang [32] developed a new approach to simulate the leached depth of cement pastes with different ionic strengths by coupling the mass transport with chemical kinetics and thermodynamic equilibria. The modelling is based on PNP equations. The modified Davies' model was

used to calculate the chemical activity. According to [36], this model is valid for concentrated solutions of ionic strengths ranging from 0 to 1.2 M, while the portlandite dissolution kinetics were calculated with the Arrhenius and Eyring equations. In this sense, Tran et al. [33,34] proposed a chloride transport model that takes into account the thermodynamic equilibria and kinetic control in order to predict chloride binding in concrete. Finally, Guo et al. [35] developed a multispecies model of chloride transport through partially saturated concrete, including the physicochemical interactions of the hydrates-pore solution. The thermodynamic coupling was based on surface complexation reactions and the dissolution/precipitation of portlandite (CH), monosulfoaluminates (AFm), ettringite (AFt) and Friedel's salt. The other salts formed during chloride transfer, such as Kugel's salt, are not considered.

The studies cited above highlight the need to include thermodynamic coupling in the modelling of reactive chloride transport. Moreover, the proposed models are based on a limited number of ions, whose concentrations are considered significant: Cl^-, Na^+, K^+ and OH^-, i.e., the divalent ions such as calcium and the sulfates are neglected even if their concentrations are not negligible compared to the previous ions [37,38]. Or, the models are based on Fick's law, which misdescribes the chloride ion transport even if they integrate all ions of the pore solution and the solid–solution interactions (thermodynamic equilibria). Those based on PNP equations do not consider the real ionic composition of the pore solution.

This paper proposes a physico-chemical multispecies modelling of reactive chloride transport through cementitious materials based on thermodynamic equilibria, which describe the dissolution/precipitation phenomena (portlandite dissolution and precipitation of minerals based on chlorides and sulfates, namely Friedel's and Kugel's

salts, AFm and AFt). The simulations highlight the concentration profiles of seven ions of the pore solution (i.e., Cl^-, Na^+, K^+, Ca^{2+}, SO_4^{2-}, $Al(OH)_4^-$ *and* OH^-) considering the multispecies reactions during chloride transport under an electrical field. The fluxes were calculated by the Nernst-Planck equation, including the diffusion and migration phenomena. The model was applied on cement pastes based on Portland cement and blast furnace slag submitted to chloride migration. For this purpose, two migration tests were considered: the migration test in the steady state [18] and the NT Build test in the non-steady state [39]. Both tests are based on seawater in the upstream compartment of the migration cell and the synthetic pore solution of the material tested in the downstream. Note that thermogravimetry analyses (TGA), pore solution extractions and scanning electron microscopy in environmental mode (E-SEM) were performed on the samples tested, before and after the migration test, in order to provide input data, determine initial conditions and monitor the dissolution/precipitation reactions during the migration test.

2. Coupling of reactive transport modelling and thermodynamic equilibria

2.1. Modelling principle

The multispecies approach proposed describes the ionic diffusion under a concentration gradient and migration induced by an external electrical field. It considers the monovalent and divalent ions of the pore solution. The modelling of the dissolution/precipitation of minerals (solid phases) in the pores during chloride transfer has also been included. The coupling is based on a pure thermodynamic approach using kinetic laws and the thermodynamic equilibrium constants (K_m) of the minerals (m) being considered [40–47]: Friedel's salt (FS), Kugel's salt (KS), portlandite (CH), monosulfoaluminates (AFm) and ettringite (AFt). The precipitated phases in the pores

depend on the ionic concentrations of the pore solution, which change during the reactive chloride transport. It should be noted that in this study, only the dissolution and leaching of portlandite is considered, without C-S-H dissolution, which occurs only with difficulty given that its composition is comprised of many varieties of calcium silicate hydrates (compounds of the ternary system CaO-SiO_2-H_2O) with complex chemical compositions [43]. During the chloride transport, portlandite is consumed, giving rise to salt formation (oxychlorides, etc) [16]. The fluxes (j_i) are calculated by the Nernst-Planck equation (Eq. 1), which considers both the diffusion and migration of species. The chemical activity is considered to be negligible. This parameter is only relevant for unsaturated conditions and it has a weak effect in the case of saturated conditions [18,36,48]. The convection is also neglected since the modelling is considered for a saturated state of the materials.

$$j_i = -D_i grad(C_i) - \frac{D_i z_i F}{RT} C_i \, grad(\Psi) \tag{1}$$

where D_i [$m^2.s^{-1}$], C_i [$mol.m^{-3}$], and z_i are the diffusion coefficient, the concentration and the valence of the ion i, respectively. F [$C.mol^{-1}$] is the Faraday constant, R [$J.mol^{-1}.K^{-1}$] is the perfect gas constant, T [K] is the absolute temperature and Ψ [V] is the total electrical potential.

In order to describe the evolution in concentrations C_i during chloride transfer, ion fluxes are used in the mass balance equation (Eq. 2).

$$\frac{\partial C_i}{\partial t} + \frac{\partial \left((1-\varphi) C_{i,b}\right)}{\partial t} = -\, div\,(j_i) + q_i \tag{2}$$

where φ is the total porosity of the material and $C_{i,b}$ is the concentration of the ion i bonded to the cement matrix. $C_{i,b}$ varies as function of the ion i concentration in the pore

solution (C_i) and is usually described by a binding isotherm : a Linear, Freundlich or Langmuir isotherm as described in the literature [21,48]. In a first approach, $C_{i,b}$ is simulated by a linear isotherm. Despite the criticism of this law, it was shown that it remains valid for modelling chemical chloride fixing by anhydrous cement [21]. The mass exchange term (q_i), added to the mass balance equation, describes the ion gain/loss in the pore solution due to the dissolution/precipitation reactions, which constitutes an originality in the proposed model. We divided it into two parts:

- Dissolution (+): it describes the concentration gain of the considered ion (Ca^{2+}) due to portlandite dissolution.
- Precipitation (−): it describes the participation of the ion in the mineral formation (Friedel's and Kugel's salts, AFm and AFt). It results in a loss of the considered ion concentration in the pore solution. More details are given in the following section.

2.2. Thermodynamic equilibrium

2.2.1. Dissolution/precipitation reactions during chloride transport

During chloride transfer, the chemical balance of the pore solution, initially in equilibrium, is disturbed from the thermodynamic point of view [16,35]. The solution tends to rebalance itself by multispecies interactions and/or exchanging ions with hydrates. This is generally reflected by reactions such as portlandite dissolution and mineral precipitation in the pores: Friedel's and Kugel's salts, AFm, AFt, etc [10,33–35]**.** The reactions depend on the phase solubility products and thermodynamic equilibria. The latter are calculated by the mass action law [8,43]. Damidot and Glasser [40] have studied the thermodynamic equilibrium of CaO-Al_2O_3-$CaCl_2$-H_2O, CaO-$CaCl_2$-H_2O and CaO-Al_2O_3-$CaSO_4$-$CaCl_2$-H_2O systems and identified the stability of the solid phases containing

chlorides and sulfates. We built on these results for coupling chloride transfer with thermodynamic equilibria (dissolution/precipitation reactions). Firstly, we integrated the precipitation of Friedel's and Kugel's salts. The latter are considered to be the main precipitated salts in cementitious materials exposed to chlorides [13,49]. Their precipitation reactions are shown in Eqs. (3) and (4), respectively [40,50].

$$4Ca^{2+} + 2Al(OH)_4^- + 2Cl^- + 4OH^- + 4H_2O \rightarrow 3CaO.Al_2O_3.CaCl_2.10H_2O \quad (3)$$

$$4Ca^{2+} + 2AlO_2^- + Cl^- + 0.5SO_4^{2-} + 4OH^- + 10H_2O \rightarrow Ca_4.Al_2(SO_4)_{0.5}.Cl(OH)_{12}.6H_2O \quad (4)$$

In addition, the dissolution of portlandite and the precipitation of AFm and AFt are considered in the proposed multispecies modelling. All of the activity products and the equilibrium constants (K_m) of the considered minerals are presented in Table 1. The equilibrium is obtained when the mineral activity product reaches the K_m value. Note that $\{...\}^n$ is the ion chemical activity to the power of the stoichiometric number n.

Table 1

Minerals considered for the dissolution/precipitation reactions.

Minerals	Chemical description	Activity products	$-\log K_m$
FS [40]	$3CaO.Al_2O_3.CaCl_2.10H_2O$	$\{Ca^{2+}\}^4 \times \{Al(OH)_4^-\}^2 \times \{OH^-\}^4 \times \{Cl^-\}^2 = K_{FS}$	29.1
KS [34]	$Ca_4.Al_2(SO_4)_{0.5}.Cl(OH)_{12}.6H_2O$	$\{Ca^{2+}\}^4 \times \{AlO_2^-\}^2 \times \{OH^-\}^4 \times \{Cl^-\} \times \{SO_4^{2-}\}^{0.5} = K_{KS}$	73.2
AFm [44]	$3CaO.Al_2O_3.CaSO_4.12H_2O$	$\{Ca^{2+}\}^4 \times \{Al(OH)_4^-\}^2 \times \{OH^-\}^4 \times \{SO_4^{2-}\} = K_{AFm}$	29.3
AFt [44]	$3CaO.Al_2O_3.3CaSO_4.32H_2O$	$\{Ca^{2+}\}^6 \times \{Al(OH)_4^-\}^2 \times \{OH^-\}^4 \times \{SO_4^{2-}\}^3 = K_{AFt}$	44.0
CH [15]	$Ca(OH)_2$.	$\{Ca^{2+}\} \times \{OH^-\}^2 = K_{CH}$	5.2

2.2.2. Dissolution and precipitation rates

During the thermodynamic imbalance, such as in the case of concrete submitted to chloride migration, the rate of mineral dissolution/precipitation depends on the kinetic constant (χ_m) [mol.m^{-2}.s^{-1}] of the mineral m and the reactive specific surface A_m [m^2.kg^{-1}], as shown by Steefel et al. [51]. The rates (r_m) are calculated by the rate law (Eq. 5)

suggested by Lasaga et al. [52]. The rate treatment of the interactions between the species and the mineral, leading to mineral dissolution/precipitation during chloride transfer, is the most general approach used for reactive transport modelling [33,34,47]. That is why we have used the same approach for coupling chloride transport and thermodynamic equilibria considering the monovalent and divalent ions of the pore solution.

$$r_m = \chi_m A_m (1 - \Omega_m) \tag{5}$$

where Ω_m is the saturation ratio of the mineral m; it can be calculated by Eq. (6) for an equilibrium state different than that giving the activity product K_m. All of the kinetic constants (χ_m) and specific reactive surface areas A_m are given in Table 2. For A_m values that had not been given in the literature, only χ_m is considered. Due to the lack of data about the kinetic constants of the precipitation of salts, Tran et al. [33,34] assumed that Kugel's salt reacts instantaneously during the chloride diffusion. For this work, we propose a parametric study of the sensitivity of the proposed model to the kinetic constants arbitrarily assumed in the literature, mainly for the kinetics of Friedel's and Kugel's salts during chloride migration under an electric field.

Table 2

Kinetic constants χ_m and specific reactive surface areas A_m of minerals.

Phases & Ref.	χ_m [mol.m^{-2}.s^{-1}]	A_m [m^2.kg^{-1}]
FS [33,34]	instantaneous	–
KS [33,34]	instantaneous	–
AFm [44]	6.8E–12	5.7E3
AFt [44]	7.1E–13	9.8E3
CH [17]	1.0E – 4 (in average)	–

Note that the mineral equilibrium is controlled by the saturation index IS_m presented in Eq. (7).

$$\Omega_m = K_m^{-1} \prod_{i=1}^{N_i} \{C_i\}^n \tag{6}$$

$$IS_m = \log \Omega_m \tag{7}$$

where m refers to FS, KS, AFm, AFt or CH; N_i is the corresponding ion i that is involved in the dissolution or precipitation. In the equilibrium state, IS_m = 0. The solution is super-saturated if IS_m < 0 and vice versa.

All of the rates (r_m) of the dissolution/precipitation reactions considered for the multispecies transport modelling are presented in Eqs. (8) to (12).

$$r_{FS} = \chi_{FS} A_{FS} \left(1 - \frac{\log(\{Ca^{2+}\}^4 \times \{Al(OH)_4^-\}^2 \times \{OH^-\}^4 \times \{Cl^-\}^2)}{\log K_{FS}}\right) \tag{8}$$

$$r_{KS} = \chi_{KS} A_{KS} \left(1 - \frac{\log(\{Ca^{2+}\}^4 \times \{AlO_2^-\}^2 \times \{OH^-\}^4 \times \{Cl^-\} \times \{SO_4^{2-}\}^{0,5})}{\log K_{KS}}\right) \tag{9}$$

$$r_{AFt} = \chi_{AFt} A_{AFt} \left(1 - \frac{\log(\{Ca^{2+}\}^6 \times \{Al(OH)_4^-\}^2 \times \{OH^-\}^4 \times \{SO_4^{2-}\}^3)}{\log K_{AFt}}\right) \tag{10}$$

$$r_{AFm} = \chi_{AFm} A_{AFm} \left(1 - \frac{\log\left(\{Ca^{2+}\}^4 \times \{Al(OH)_4^-\}^2 \times \{OH^-\}^4 \times \{SO_4^{2-}\}\right)}{\log K_{AFm}}\right) \quad (11)$$

$$r_{CH} = \chi_{CH} A_{CH} \left(1 - \frac{\log\left(\{Ca^{2+}\} \times \{OH^-\}^2\right)}{\log K_{CH}}\right) \quad (12)$$

3. Case studies

The proposed model makes it possible to simulate the concentration profiles of all the pore solution ions of cementitious materials submitted to lab chloride migration under an electrical field, including the interactions involved during the multispecies transport. For this study, two migration tests are simulated:

- The chloride migration test in a steady state: in order to simulate a real exposure to seawater, the test is based on seawater at the upstream compartment and the synthetic pore solution of the material tested at the downstream. The solution concentrations were maintained constant during the test by daily renewals of the compartment solutions. An electrical field of 300 $V.m^{-1}$ was applied between the two sides of the sample tested (with 0.05 m thickness) in order to accelerate the chloride penetration [18,53,54].
- NT Build 492 test in a non-steady state: the test is based on the same compartment solutions and electrical field as the migration test in a steady state. However, NT Build 492 test is only used in a non-steady state, where the chloride migration coefficient is determined from the depth of the chloride penetration in the sample [39]. The latter is obtained by spraying the split face of the sample tested with $AgNO_3$, which reacts with the chlorides to form a distinct boundary depicting the limit of the chloride penetration through the sample.

Simulations concern two cement paste compositions: an ordinary Portland cement paste called CP (water to binder "W/B" ratio of 0.5) and a slag cement paste with a mass substitution of 75% of Portland cement by a blast furnace slag called BFS75 (W/B of 0.44). The chemical compositions of the cement CEM I 52.5 N and slag used are given in Table 3. The paste properties obtained from experimental investigations are used as input data for the modelling [14,17]. Further information is given below.

Table 3

Compositions of the cement and slag used.

Composition	CaO	SiO_2	Al_2O_3	Fe_2O_3	SO_3	K_2O	Na_2O	Chlorides
CEM I (wt.%)	64.20	20.50	5.00	3.90	2.50	0.29	0.05	1.40
Slag (wt.%)	41.50	33.30	12.50	0.40	0.50	0	0	0

3.1. System of equations and mathematical solution

The multispecies mathematical modelling proposed is presented in the system of Eqs. (13). The model considers the diffusion and migration under an applied electrical field E (300 $V.m^{-1}$) for the flux calculation using the Nernst-Planck equation. The local electrical field is neglected in front of the external one applied for the migration test [18]. Also, chloride chemical binding is considered as explained in section 2.1. The mineral rate (r_m) is multiplied by a factor representing the stoichiometric number ($n_{i,m}$) of each ion i and mineral m with a positive sign (ion gain in the pore solution) and a negative sign (ion loss) as described in section 2.1. The mineral rates, calculated by using Eqs. 8 to 12, and stoichiometric numbers are replaced in Eq. 13 to calculate the mass exchange term (q_i) of the corresponding ion (see Eqs. 2 and 13). Note that in this approach based on ionic concentrations, we did not integrate the ion transference numbers, which point out the proportion of the current carried by a given ion to the global current of ions during the chloride migration test [55,56].

$$\begin{cases} \dfrac{\partial C_{Cl}}{\partial t} + (1-\varphi)\dfrac{\partial C_{Cl,b}}{\partial t} = -\,div\,(j_{Cl}) - n_{Cl,FS} \times r_{FS} - n_{Cl,KS} \times r_{KS} \\ \dfrac{\partial C_{Na}}{\partial t} = -div\,(j_{Na}) \\ \dfrac{\partial C_{K}}{\partial t} = -div\,(j_{K}) \\ \dfrac{\partial C_{Ca}}{\partial t} = -\,div\,(j_{Ca}) + n_{Ca,FS} \times r_{CH} - n_{Ca,FS} \times r_{FS} - n_{Ca,KS} \times r_{KS} - n_{Ca,AFt} \times r_{AFt} - n_{Ca,AFm} \times r_{AFm} \\ \dfrac{\partial C_{SO4}}{\partial t} = -div\,(j_{SO4}) - n_{SO4,KS} \times r_{KS} - n_{SO4,AFt} \times r_{AFt} - n_{SO4,AFm} \times r_{AFm} \\ \dfrac{\partial C_{Al}}{\partial t} = -div\,(j_{Al}) - n_{Al,FS} \times r_{FS} - n_{Al,KS} \times r_{KS} - n_{Al,AFt} \times r_{AFt} - n_{Al,AFm} \times r_{AFm} \\ j_i = -D_i grad(C_i) + \dfrac{D_i z_i FE}{RT} C_i \end{cases} \quad (13)$$

3.2. Required input data and initial conditions: experimental characterization

3.2.1. Porosity and ion diffusion coefficients

In order to provide input data for the multispecies model proposed, the intrinsic parameters (porosity and ion diffusion coefficients) of CP and BFS75 were measured. Cylindrical specimens (11 cm in diameter and 22 cm thick) of cement pastes CP and BFS75 were manufactured. Next, the surfaces were immediately covered with a cellophane film in order to avoid cracks due to the water evaporation and shrinkage. 24 hours later, the specimens were cured in an alkaline solution of 25 mM NaOH and 83 mM KOH for one year (365 days) until sampling [57,58]. Cement pastes have been chosen to guarantee the representativeness of the samples and to avoid the heterogeneity that an aggregate would induce, especially during chemical analyses. Afterwards, the water porosities "φ" were measured by hydrostatic weighing according to the French NFP 18-459 standard (Table 4).

Moreover, the effective diffusion coefficients of the different ions were calculated using Eq. (14) based on the ionic diffusion coefficient of the species i in water "$D_{i,w}$" and the formation factor "f". The calculation of the formation factor depends on the geometrical parameters of the material's microstructure: porosity "φ" and tortuosity "τ", according

to [59,60] (see Eq. 14). The parameter related to the electrical double layer is neglected considering: (i) high ionic concentrations involved during ion transfer in the sample's pore solution; and (ii) the coarse porosity and pore diameter of the pastes tested (average > 8 nm [14]). Indeed, electrocapillary phenomena governing electrical double layer could be neglected in this case [15,33,35,61]. Formation factors and ionic diffusion coefficients obtained are in agreement with those given by the literature [9,26,62–64] (see Table 4).

$$D_{i,eff} = f \times D_{i,w} = \varphi \times \tau \times D_{i,w} \quad (14)$$

where $D_{i,w}$ at 25°C were obtained from the literature [65].

Table 4

Porosities and ionic diffusion coefficients of the materials tested (CP and BFS75).

Material	φ [%]	f ($x10^{-3}$)	D_{Cl} [$x10^{-12}$ m^2 s^{-1}]	D_{Na} [$x10^{-12}$ m^2 s^{-1}]	D_k [$x10^{-12} m^2 s^{-1}$]	D_{Ca} [$x10^{-12}$ m^2 s^{-1}]	D_{SO_4} [$x10^{-12}$ m^2 s^{-1}]	$D_{Al(OH)_4}$ [$x10^{-12}$ m^2 s^{-1}]
CP	34	4.42	8.72	5.71	8.42	3.41	4.60	2.40
BFS75	29	1.74	3.72	2.44	3.59	1.45	1.96	1.02

3.2.2. Pore solution extraction

The assessing of the initial conditions of the proposed modelling required analyses of the initial pore solution of the tested materials, i.e., before exposure to chlorides. For this purpose, the pore solutions of CP and BFS75 were extracted by pressing as per the method described by Barneyback and Diamond [66]. The amount of the pore solution extracted was of about 8 ml. The efficiency of the extraction technique used and the representativity of the solution extracted are highlighted in [38,66]. Afterwards, the solutions were analyzed by Ionic Chromatography. The chemical composition of pore solutions of healthy CP and BFS75 are given in Table 5. Given the cement aluminum content, we assume in the numerical modelling that the presence of $Al(OH)_4^-$ in the pore

solution is sufficient to cause mineral precipitations during chloride migration.

Table 5

Chemical composition of CP and BFS75 pore solutions before the migration test.

	Na^+	K^+	Cl^-	Ca^{2+}	SO_4^{2-}	$Al(OH)_4^-$	OH^-
CP (mM)	51	117	4	2	2	6	158
BFS75 (mM)	48	51	3	2	2	6	90

In general, the results confirm that the pore solutions of CP and BFS75 are mainly composed of sodium and potassium. The divalent ion concentrations are relatively significant and cannot be neglected. Blast furnace slag used for this study did not contain sodium oxide and potassium oxide as shown in Table 3, which explains the low concentrations of Na^+ and K^+ in BFS75 compared to CP.

3.2.3. Monitoring of the dissolution/precipitation reactions

In order to confirm the possible dissolution/precipitation reactions that may occur during chloride migration, elemental distribution of the solid phases at the microscopic level was performed on healthy CP and BFS75 and others submitted to the migration test (up to the steady state) by using scanning electron microscopy in environmental mode (E-SEM). Analyses were performed using an FEI Quanta 200 Environmental Field Effect Gun apparatus equipped with an EDAX-Genesis EDS and operated in the range of 3.5–20 kV accelerating voltage. The advantage of the E-SEM technique is that no surface polishing is required and no coverage is deposited on the surface of the examined sample, which preserves its morphology and microstructure [67]. SEM images of CP and BFS75 and the corresponding EDX spectra are shown in Figs. 1 and 2. We are interested in the chloride amount of the analyzed solid phase of the contaminated paste (samples having undergone the migration test): +2.4% wt for CP and +1.2% wt for BSF75. These Cl-amounts participate in the precipitation of Friedel's salt and/or Kugel's salt. This

finding will be considered in the following proposed multispecies transport modelling. The amounts of aluminum and sulfur precipitated were 2.1% wt and 1.1% wt, respectively, for CP and 3.5% wt and 0.4% wt for BFS75. Al and S are integrated into the precipitation of the minerals KS, AFm and AFt. However, the Ca experimental monitoring remains difficult because of its presence in all the considered minerals and its release from the portlandite during the chloride migration under the electrical field [16,68].

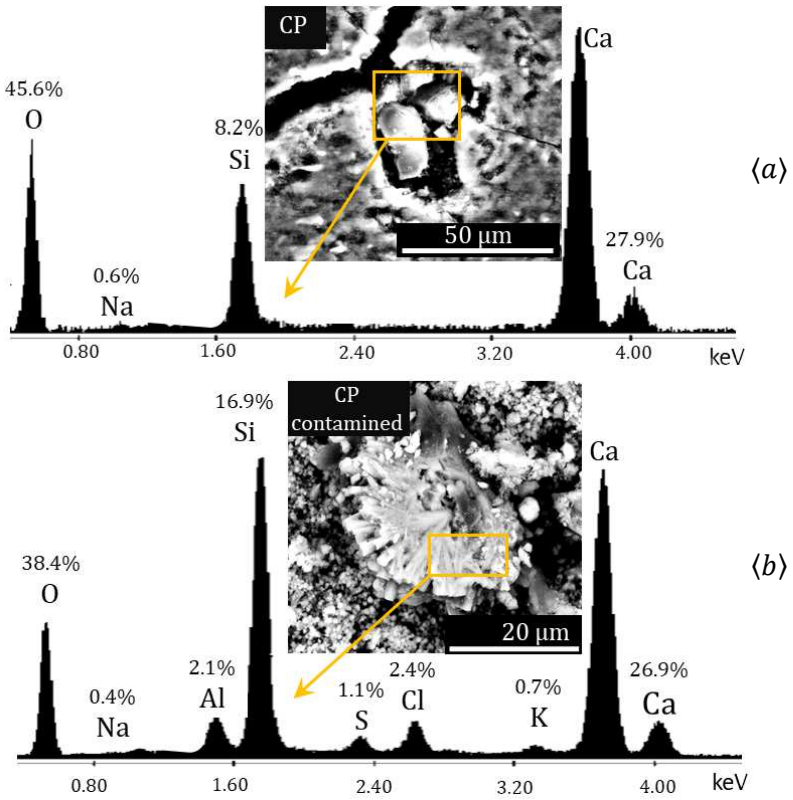

Fig. 1. E-SEM images and EDX spectra of CP solid phase ⟨***a***⟩ before and ⟨***b***⟩ after chloride migration test.

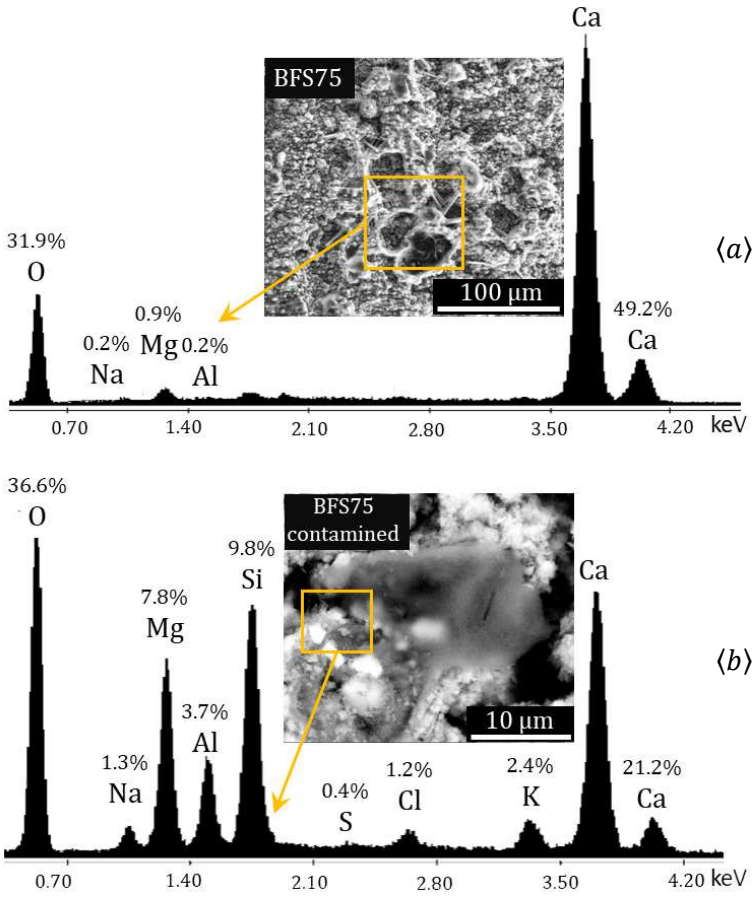

Fig. 2. E-SEM images and EDX spectra of BFS75 solid phase ⟨***a***⟩ before and ⟨***b***⟩ after chloride migration test.

Moreover, we have quantified the portlandite in both materials tested using a thermogravimetric analysis (TGA). TGA allows the monitoring of the mass variation of the material tested versus the temperature and the determination of the material components. For good reproducibility, analyses were performed on three powder samples of 112 ± 7 mg obtained from ground cement pastes. In order to avoid any possible carbonation, the powders were immediately analyzed after grinding using a Setaram Setsys Evolution® device with a heating rate of 10 °C/min from 20 to 1000 °C [3]. TG and derivative TG (DTG) curves are shown in Fig. 3. The portlandite amount (*CH*) was calculated from the mass loss between the tangents of the TG curve at temperatures T1 ≈ 420°C and T2 ≈ 530 °C according to, [69,70] (see Eq. 15).

$$CH = \frac{\Delta m_{T_1 \to T_2}}{m_s} \times \frac{\rho_s}{M_{H_2O}} \quad (15)$$

where CH [mol.m^{-3}] is the portlandite amount, $\Delta m_{T_1 \to T_2}$ [kg] is the mass loss of the sample tested between T_1 and T_2, m_s [kg] is the sample mass, ρ_s [kg.m^{-3}] is the sample density and M_{H_2O} [kg.mol^{-1}] is the molecular weight of H_2O.

The average obtained amounts of portlandite are about 6195 ± 438 mol.m^{-3} of CP and 1491 ± 186 mol.m^{-3} of BFS75. These amounts of portlandite will be compared to the dissolved portlandite obtained from the simulations given below in order to confirm the availability of portlandite throughout the migration test (i.e., maintaining the dissolution of portlandite until the end of the test), mainly for BFS75, where portlandite is consumed to form C-S-H due to pozzolanic effects [71].

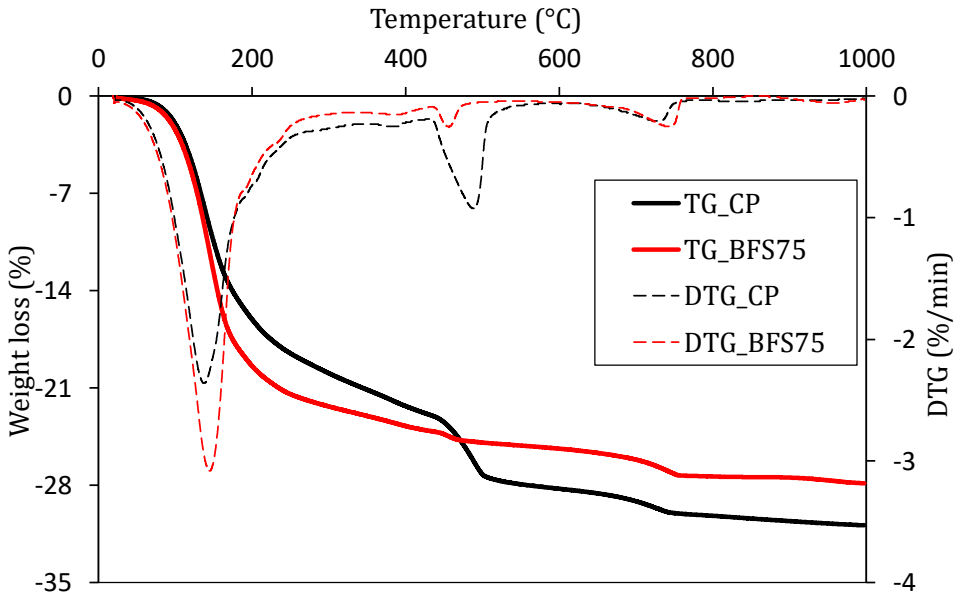

Fig. 3. TG/DTG curves of CP and BFS75.

Finally, input data and the initial/boundary conditions required for the proposed modelling of the migration test at the steady state, for the two materials CP and BFS75, are summarized in Tables 6–8. Dirichlet boundary conditions were used, which reflect the regular renewal of the compartment solutions during the standard migration test.

Note that the same input data and initial and boundary conditions were used for the modelling of the NT Built 492 test. Except for the anodic sample side (downstream, x=L), the Neumann boundary condition is considered.

Table 6

Input data for the proposed modelling.

Symbol	Parameter	Value (unity)
R	Perfect-gas constant	8.314 (J. K^{-1}. mol^{-1})
F	Faraday's constant	96500 (C. mol^{-1})
E	Electrical field	300 (V. m^{-1})
φ	Total porosity	Table 4
D_i	Effective diffusion coefficient of ion i	Table 4
a	Linear isotherm constant	{CP: 7.48 [72]; BFS75: 1.5 [73]}
K_m	Mineral *m* equilibrium constant	Table 1
$\chi_{FS,\ KS}$	Mineral *m* kinetic constant of FS; KS; CH	Parametric study
$X_{AFt,\ AFm\ or\ CH}$	Mineral *m* kinetic constant of AFt or AFm	Table 2

Table 7

Initial and boundary conditions used for CP.

Boundary conditions		Initial conditions
(upstream, seawater [74]) (x=0, t) [mol. m^{-3}]	(downstream, CP pore solution) (x=L, t) [mol. m^{-3}]	(CP pore solution) (t=0, 0<x<L) [mol. m^{-3}]
$\begin{cases} C_{Cl^-} = 565 \\ C_{Na^+} = 485 \\ C_{K^+} = 11 \\ C_{Ca^{2+}} = 11 \\ C_{SO_4^{2-}} = 29 \\ C_{Al(OH)_4^-} = 4 \\ C_{OH^-} = 1 \end{cases}$	$\begin{cases} C_{Cl^-} = 4 \\ C_{Na^+} = 51 \\ C_{K^+} = 117 \\ C_{Ca^{2+}} = 2 \\ C_{SO_4^{2-}} = 2 \\ C_{Al(OH)_4^-} = 6 \\ C_{OH^-} = 158 \end{cases}$	$\begin{cases} C_{Cl^-} = 4 \\ C_{Na^+} = 51 \\ C_{K^+} = 117 \\ C_{Ca^{2+}} = 2 \\ C_{SO_4^{2-}} = 2 \\ C_{Al(OH)_4^-} = 6 \\ C_{OH^-} = 158 \end{cases}$

Table 8

Initial and boundary conditions used for BFS75.

Boundary conditions		Initial conditions
(upstream, seawater [74]) (x=0, t)	(downstream, BFS75 pore solution) (x=L, t)	(BFS75 pore solution) (t=0, 0<x<L)

[mol. m^{-3}]	[mol. m^{-3}]	[mol. m^{-3}]
$\begin{cases} C_{Cl^-} = 565 \\ C_{Na^+} = 485 \\ C_{K^+} = 11 \\ C_{Ca^{2+}} = 11 \\ C_{SO_4^{2-}} = 29 \\ C_{Al(OH)_4^-} = 4 \\ C_{OH^-} = 1 \end{cases}$	$\begin{cases} C_{Cl^-} = 1 \\ C_{Na^+} = 48 \\ C_{K^+} = 51 \\ C_{Ca^{2+}} = 1.5 \\ C_{SO_4^{2-}} = 2 \\ C_{Al(OH)_4^-} = 6 \\ C_{OH^-} = 91 \end{cases}$	$\begin{cases} C_{Cl^-} = 1 \\ C_{Na^+} = 48 \\ C_{K^+} = 51 \\ C_{Ca^{2+}} = 1.5 \\ C_{SO_4^{2-}} = 2 \\ C_{Al(OH)_4^-} = 6 \\ C_{OH^-} = 91 \end{cases}$

3.3. Numerical results and discussion

The simulations of the ion concentration profiles of CP and BFS75 submitted to a chloride migration test until reaching the steady state are given in Figs. 4 and 5, respectively. The results show the concentration profiles, with and without considering the thermodynamic equilibria. The ion concentrations are normalized to $C_{i,0}$ at (t, x=0), i.e., corresponding to the ion *i* concentration in seawater (boundary condition).

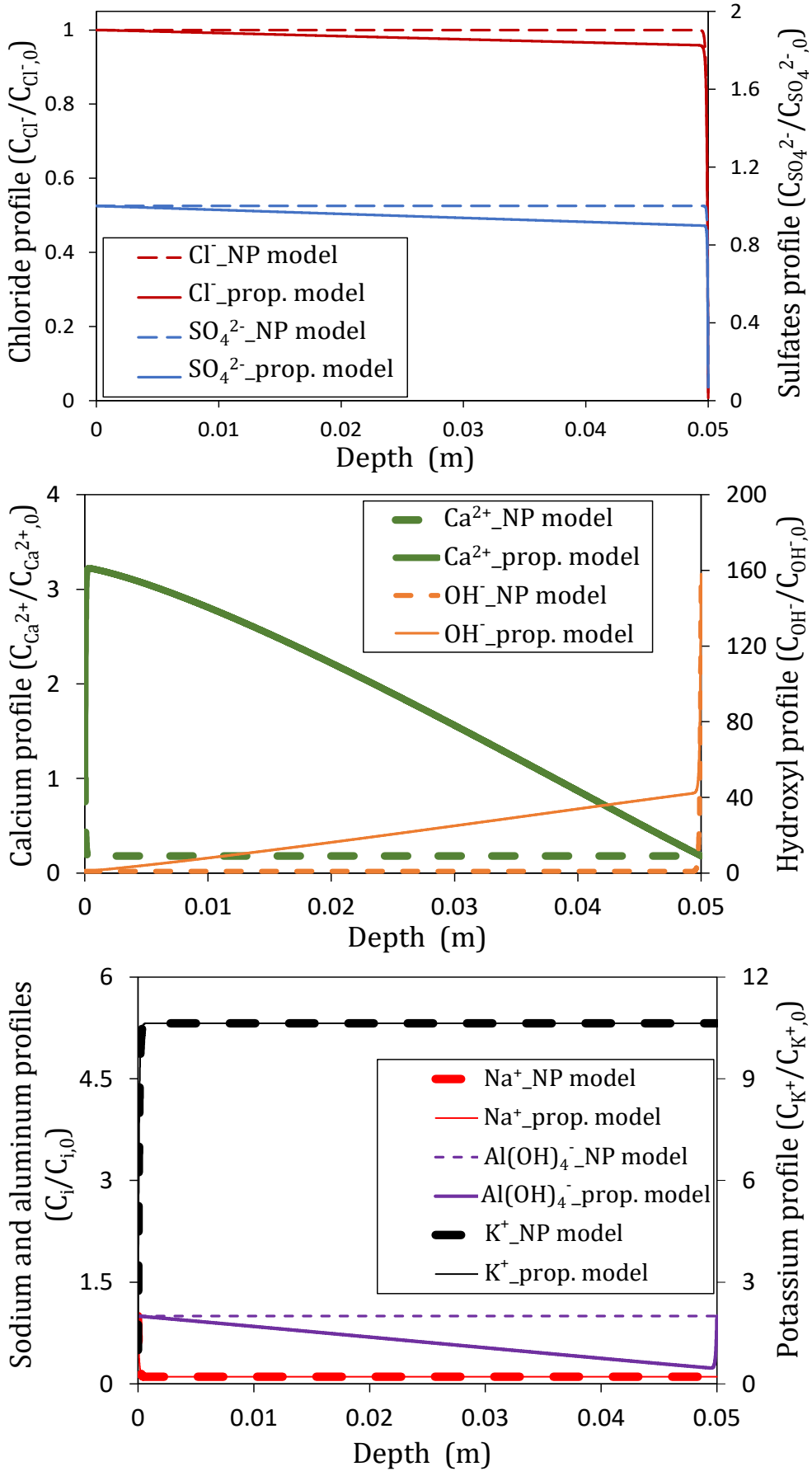

Fig. 4. Ion concentration profiles in CP simulated following a migration test at steady state using the NP model and the proposed one.

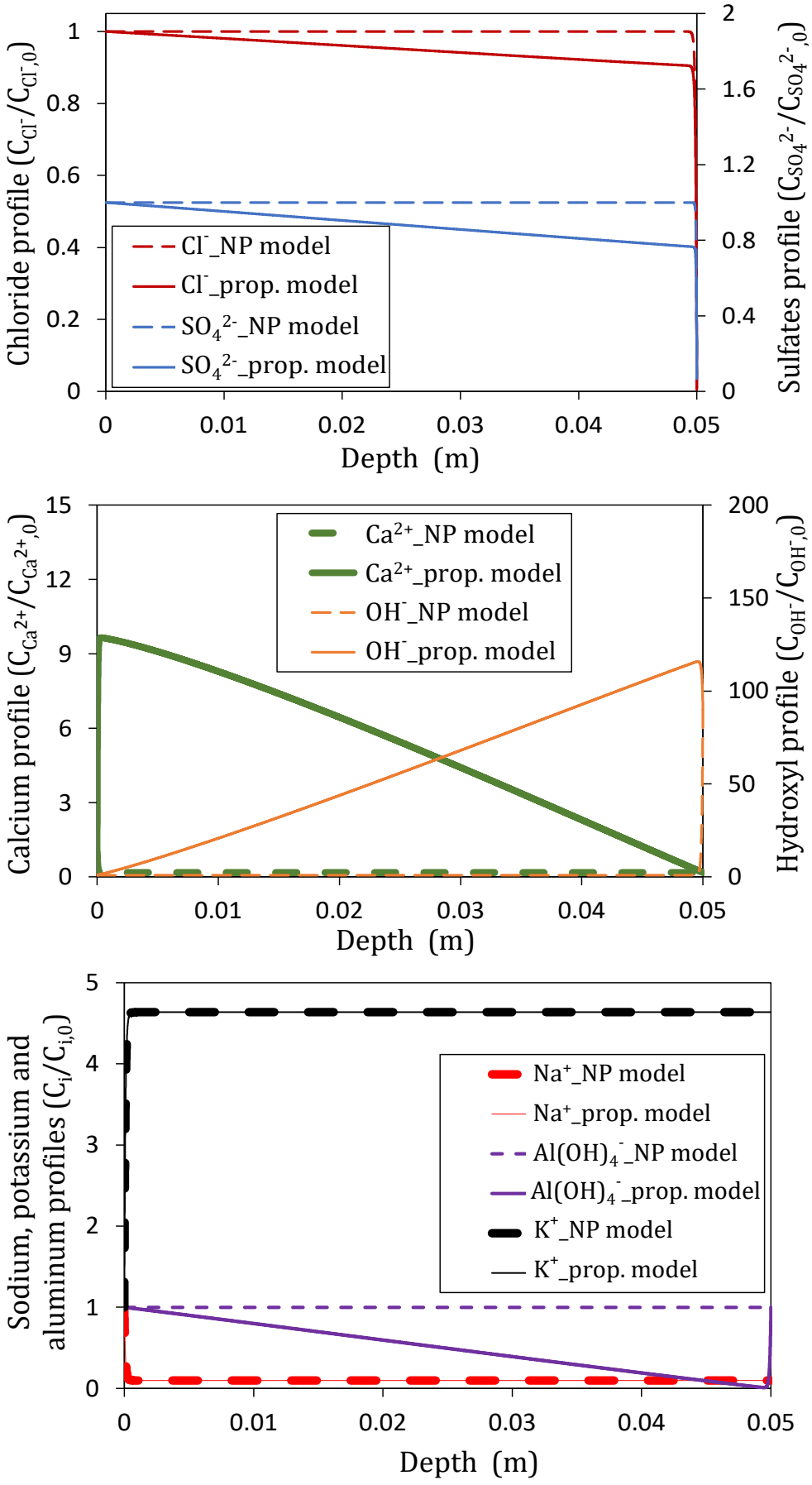

Fig. 5. Ion concentration profiles in BFS75 simulated following a migration test at steady state using the NP model and the proposed one.

The simulations show a difference between the ion profile concentrations obtained from the NP model and the proposed one. The consideration of thermodynamic equilibria in the proposed transport modelling highlights a reduction of up to 10% of chlorides, 22% of sulfates and 95% of aluminum concentrations compared to the classic NP modelling. Chlorides are consumed for the precipitation of FS and KS, sulfates are consumed for the precipitation of KS, AFm and AFt while $Al(OH)_4^-$ participates in the precipitation of all the minerals considered (FS, KS, AFm and AFt). We note that the species reductions depend on the kinetics constant χ_m of the mineral precipitation considered: χ_{AFm} = 6.8E–12 [44]; χ_{AFt} = 7.1E–13 [44]; χ_{CH} = 1.0E–4 [17] and χ_{FS} = χ_{KS} = 1.0E–5. χ_{FS} and χ_{KS} values correspond to the kinetic giving the maximum precipitation of Friedel's and Kugel's salts during chloride migration. More details are given in the following parametric study showing the sensitivity of the simulations to χ_{FS} and χ_{KS}. However, the proposed model shows that the calcium and hydroxyl concentrations are higher compared to the NP model despite their involvement in solid-phase precipitation. Both ions (Ca^{2+} and OH^-) are released by the portlandite during chloride migration [16,68]. This is promoted by the dissolution kinetics of portlandite, which are higher than those of the mineral precipitations.

In general, the proposed multispecies model coupled with thermodynamic equilibria realistically simulates all of the ion profiles in materials exposed to chloride migration under an electrical field. In fact, the NP modelling of chloride migration without considering thermodynamic equilibria overestimates the Cl^-, SO_4^{2-} and $Al(OH)_4^-$ profiles and underestimates the Ca^{2+} and OH^- profiles at steady state. Finally, the amounts of the portlandite dissolved (consumed) obtained from simulations are 104 mol.m^{-3} for PC and 358 mol.m^{-3} for BFS75. These amounts remain lower than the initial values of the

healthy pastes (available for the dissolution) before chloride migration: 6195 $mol.m^{-3}$ for CP and 1491 $mol.m^{-3}$ for BFS75 (see section 3.2.3).

Moreover, simulations of the ion concentration profiles of PC and BFS75 submitted to a 24-hour NT build 492 test at non-steady state were carried out (Figs. 6 and 7). The results showed a similarity between the chloride profiles obtained with the two models (NP and the proposed one) with a slight difference for the sulfate profiles. Despite the increase in concentration of Ca^{2+} and OH^- released from the portlandite dissolution almost instantaneously (see Figs 6 and 7), the duration of the NT Build 492 test (24 hours) is too short for Ca^{2+} and OH^- to affect the chloride profile. We note that the effect consists of the precipitation of Friedel's and Kugel's salts, involving free chlorides in the pore solution. The precipitation kinetics of these salts are too low to produce their effects on the chloride profile during 24 hours of NT Build 492 test simulated.

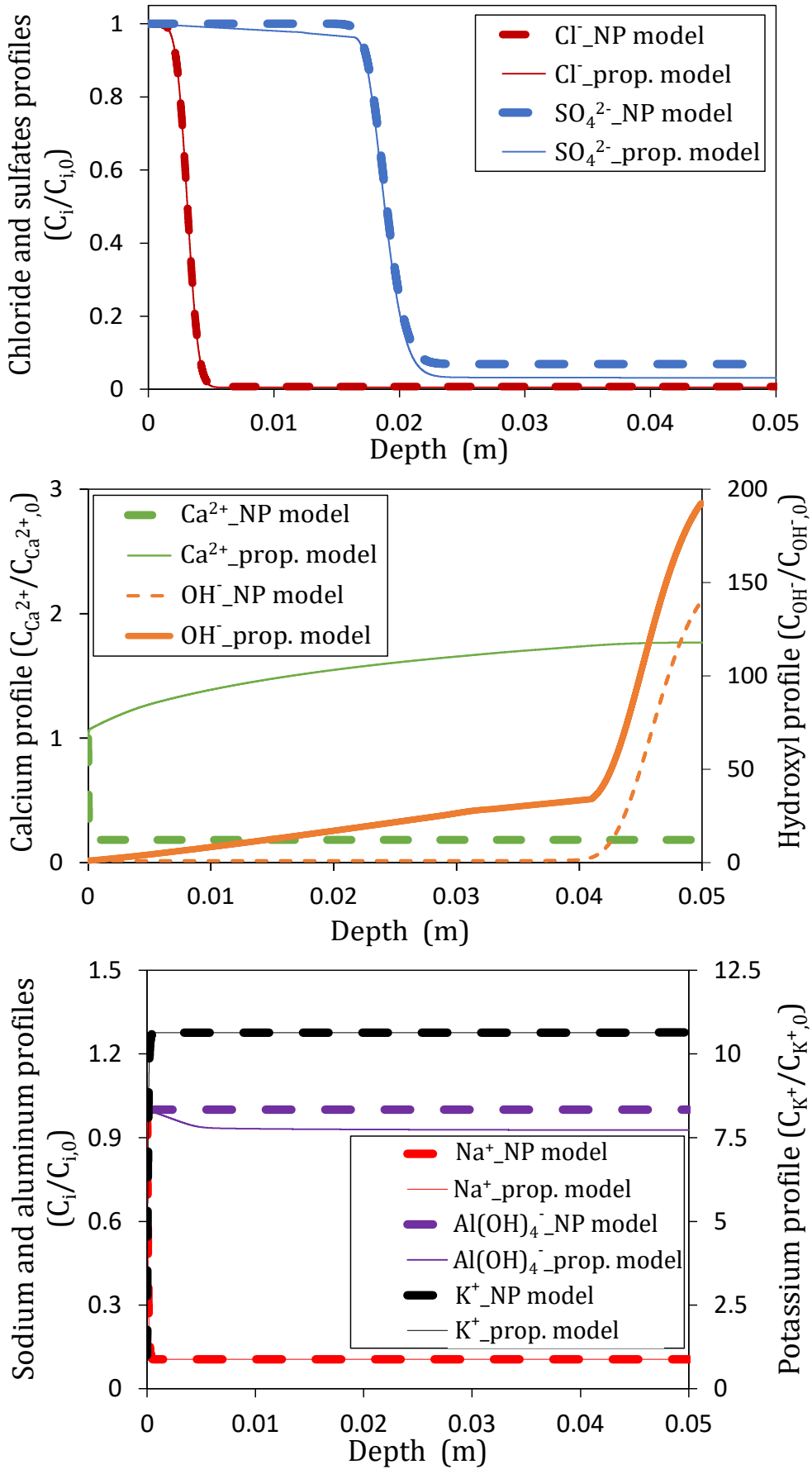

Fig. 6. Ion concentration profiles in CP simulated following 24-hour NT Build 492 test at non-steady state using the NP model and the proposed one.

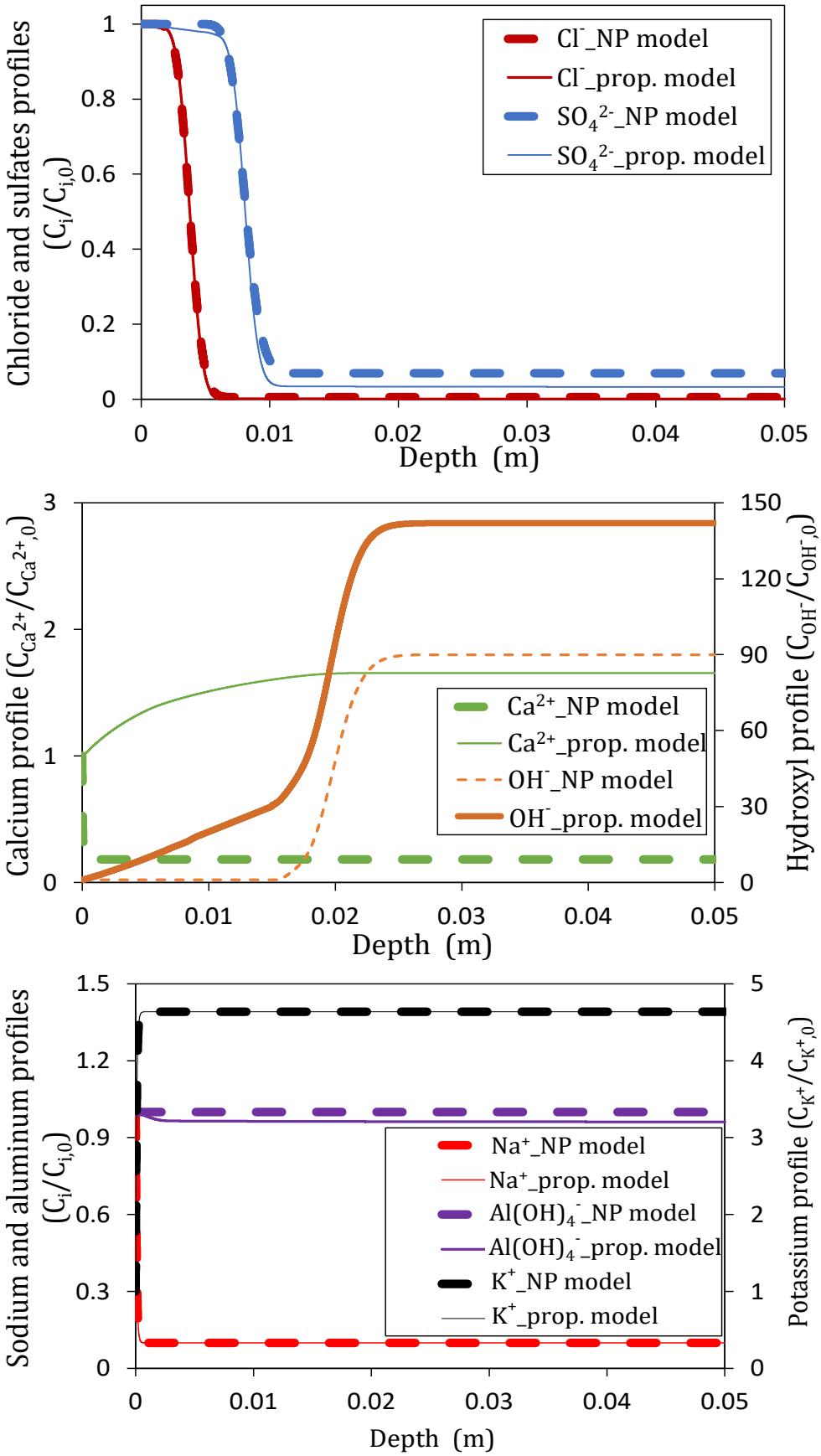

Fig. 7. Ion concentration profiles in BFS75 simulated following 24-hour NT Build 492 test at non-steady state using the NP model and the proposed one.

3.3.1. Modelling sensitivity to the kinetic constants χ_m

In order to check the sensitivity of the proposed model to the mineral kinetic constants considered (χ_m), whose values are arbitrarily assumed in the literature, we vary χ_{FS} and χ_{KS}, for the simulation of the concentration profiles of CP submitted to the migration test at steady state. Note that no research, to our knowledge, has studied these kinetic constants of the dissolution/precipitation of minerals during chloride migration. We present the results of the chloride concentration profiles with the highest sensitivity to χ_{FS} and χ_{KS} values, giving the maximum precipitation of Friedel's and Kugel's salts and vice versa for the least sensitive constants (Fig. 8). Four values are taken for χ_{FS} and χ_{KS}, which range between 1E–8 and 1E–5. These values have been chosen to consider any possible influence of salt precipitation on the ionic transfer. The other mineral kinetics are maintained as constant (see Table 2). The simulations highlight that χ_{FS} and χ_{KS} affect the chloride profiles of CP. The precipitation of these ions increases with χ_{FS} and χ_{KS} considered. An additional precipitation of 5% of chlorides was noticed for $\chi_{FS} = \chi_{KS} =$ 1E–5 compared to that obtained for the minimal kinetics ($\chi_{FS} = \chi_{KS} =$ 1E–8). Monitoring the precipitation kinetics of salts during a migration test could enhance the model in terms of the prediction of chloride profiles.

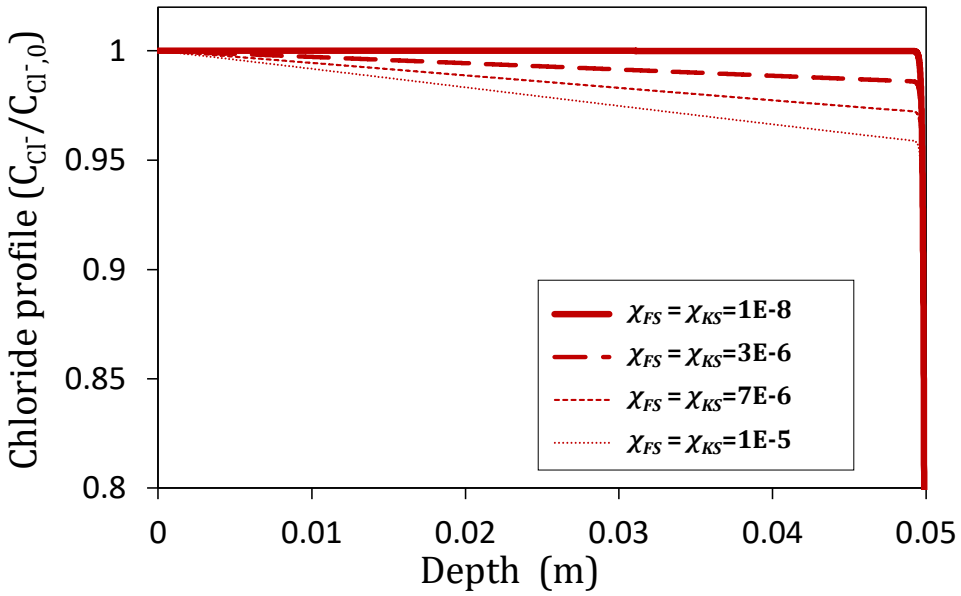

Fig. 8. Chloride profiles vs. different values of χ_{FS} and χ_{KS} in CP submitted to chloride migration test at steady state.

4. Conclusions

A multi-ionic approach for the modelling of reactive chloride transport through saturated cementitious materials is proposed. The modelling is based on coupling the NP equation and thermodynamic equilibria. The numerical results lead to the following conclusions:

- The proposed coupling of the ionic transport and thermodynamic equilibria allows the simulation of the chloride migration test based on seawater and the material pore solution at steady and non-steady states (considering all the monovalent and divalent ions). The model considers the diffusion, migration and kinetics of the minerals dissolved or precipitated. The NP modelling overestimates the free chloride concentration of the materials tested by about 10% compared to the proposed modelling. It would be interesting to test the proposed model in the case of natural diffusion in order to simulate the chloride ingress in real configurations for predicting structure service life. In addition, some form of experimental validation of the ion concentration profiles within the

sample tested would be very useful for assessing the sensitivity of the modelling parameters. This could be the subject of a future work.

- The results show that the proposed model for simulating the reactive transfer of chloride through cementitious materials is substantially dependent on the choice of kinetic constants of mineral dissolution/precipitation. The kinetics considered must therefore be carefully chosen. Experimental monitoring of these kinetics is therefore of importance in order to enrich the literature and improve the robustness of the proposed model for predicting chloride transfer.

Declarations of interest: none

Funding sources

This research did not receive any specific grant from funding agencies in the public, commercial, or not-for-profit sectors.

Acknowledgments

The authors would like to thank Dr. Egle Conforto from LaSIE UMR CNRS 7356 for the realization of SEM images, Mr. Antony Gelicus for the chemical analyses by ionic chromatography and the NEEDS-VARCIM research program and CPER-FEDER program ("Bâtiment durable", Axis 2 "MADUR") 2014–2020 for having supported this work.

5. References

[1] European Standard EN 206–1/CN, Concrete — Part 1: Specification, Performances, Production and Conformity, 2014.

[2] M. Qin, A. Aït-Mokhtar, R. Belarbi, Two-dimensional hygrothermal transfer in porous building materials, Appl. Therm. Eng. 30 (16) 2555–2562.

[3] N. Issaadi, A. Nouviaire, R. Belarbi, A. Aït-Mokhtar, Moisture characterization of cementitious material properties: Assessment of water vapor sorption isotherm and permeability variation with ages, Constr. Build. Mater. 83 (2015) 237–247.

[4] O. Poupard, A. Aït-Mokhtar, P. Dumargue, Impedance spectroscopy in reinforced concrete: procedure for monitoring steel corrosion. Part I: development of the experimental device, J. Mater. Sci. 38 (2003) 2845–2850.

[5] O. Poupard, A. Aït-Mokhtar, P. Dumargue, Impedance spectroscopy in reinforced concrete: experimental procedure for monitoring steel corrosion: part II: polarization effect, J. Mater. Sci. 38 (2003) 3521–3526.

[6] C. Li, L. Jiang, S. Li, Effect of limestone powder addition on threshold chloride concentration for steel corrosion in reinforced concrete, Cem. Concr. Res. 131 (2020) 106018.

[7] F.P. Glasser, J. Pedersen, K. Goldthorpe, M. Atkins, Solubility reactions of cement components with NaCl solutions: I. $Ca(OH)_2$ and C-S-H', Adv. Cem. Res. 17 (2005) 57–64.

[8] B. Johannesson, K. Yamada, L-O. Nilsson, Y. Hosokawa, Multi-species ionic diffusion in concrete with account to interaction between ions in the pore solution and the cement hydrates, Mater. Struct. 40 (2007) 651–665.

[9] M.M. Jensen, K. De Weerdt, B. Johannesson, M.R. Geiker, Use of a multi-species reactive transport model to simulate chloride ingress in mortar exposed to NaCl solution or sea-water, Comput. Mater. Sci. 105 (2015) 75–82.

[10] Y. Cao, L. Guo, B. Chen, J. Wu, Thermodynamic modelling and experimental investigation on chloride binding in cement exposed to chloride and chloride-sulfate solution, Constr. Build. Mater. 246 (2020) 118398.

[11] M. Castellote, C. Andrade, C. Alonso, Changes in concrete pore size distribution due to electrochemical chloride migration trials, ACI Mater. J. 96 (1999) 314–319.

[12] C. Andrade, M. Castellote, J. Sarria, C. Alonso, Evolution of pore solution chemistry, electro-osmosis and rebar corrosion rate induced by realkalization, Mater. Struct. 32 (1999) 427–436.

[13] C. Qiao, P. Suraneni, J. Weiss, Damage in cement pastes exposed to NaCl solutions, Constr. Build. Mater. 171 (2018) 120–127.

[14] R. Cherif, A. Hamami, A. Aït-Mokhtar, Global quantitative monitoring of the ion exchange balance in a chloride migration test on cementitious materials with mineral additions, Cem. Concr. Res. 138 (2020) 106240.

[15] E. Samson, J. Marchand, Modeling the transport of ions in unsaturated cement-based materials, Comput. Struct. 85 (2007) 1740–1756.

[16] L. Sutter, K. Peterson, S. Touton, T. Van Dam, D. Johnston, Petrographic evidence of calcium oxychloride formation in mortars exposed to magnesium chloride solution, Cem. Concr. Res. 36 (2006) 1533–1541.

[17] R. Cherif, A. Hamami, A. Aït-Mokhtar, Effects of leaching and chloride migration on the microstructure and pore solution of blended cement pastes during a migration test, Constr. Build. Mater. 240 (2020) 117934.

[18] C. Andrade, Calculation of chloride diffusion coefficients in concrete from ionic migration measurements, Cem. Concr. Res. 23 (1993) 724–742.

[19] O. Amiri, A. Aït-Mokhtar, A. Seigneurin, A complement to the discussion of A. Xu and S. Chandra about the paper "Calculation of chloride coefficient diffusion in concrete from ionic migration measurements" by C. Andrade, Cem. Concr. Res. 27 (1997) 951–957.

[20] E. Samson, J. Marchand, Numerical Solution of the Extended Nernst–Planck Model, J. Colloid Interface Sci. 215 (1999) 1–8.

[21] O. Amiri, A. Aït-Mokhtar, P. Dumargue, G. Touchard, Electrochemical modelling of chloride migration in cement-based materials. Part I. Theoretical basis at microscopic scale, Electrochim. Acta 46 (2001) 1267–1275.

[22] H. Friedmann, O. Amiri, A. Aït-Mokhtar, Shortcomings of geometrical approach in multi-species modelling of chloride migration in cement-based materials, Mag. Concr. Res. 60 (2008) 119–124.

[23] K. Bourbatache, O. Millet, A. Aït-Mokhtar, Ionic transfer in charged porous media. Periodic homogenization and parametric study on 2D microstructures, Int. J. Heat Mass Transf. 55 (2012) 5979–5991.

[24] K. Bourbatache, O. Millet, A. Aït-Mokhtar, O. Amiri, Modeling the chlorides transport in cementitious materials by periodic homogenization, Transp. Porous Media 94 (2012) 437–459.

[25] H. Sleiman, O. Amiri, A. Aït-Mokhtar, J.M. Loche, Chloride transport through unsaturated concrete: chloride profile simulations and experimental validation, Mag. Concr. Res. 64 (2012) 351–359.

[26] L-X. Mao, Z. Hua, J. Xia, G-L. Feng, I. Azim, J. Yang, Q-F. Liu, Multi-phase modelling of electrochemical rehabilitation for ASR and chloride affected concrete composites, Compos. Struct. 207 (2019) 176–189.

[27] D. Li, L. Li, X. Wang, Chloride diffusion model for concrete in marine environment with considering binding effect, Mar. Struct. 66 (2019) 44–51.

[28] L. Jiang, Z. Song, H. Yang, Q. Pu, Q. Zhu, Modeling the chloride concentration profile in migration test based on general Poisson Nernst Planck equations and pore structure hypothesis, Constr. Build. Mater. 40 (2013) 596–603.

[29] J. Xia, L. Li, Numerical simulation of ionic transport in cement paste under the action of externally applied electric field, Constr. Build. Mater. 39 (2013) 51–59.

[30] M. Fenaux, E. Reyes, J. C. Gálvez, A. Moragues, Modelling the transport of chloride and other ions in cement-based materials', Cem. Concr. Compos. 97 (2019) 33–42.

[31] M.M. Jensen, B. Johannesson, M.R. Geiker, Framework for reactive mass transport: Phase change modeling of concrete by a coupled mass transport and chemical equilibrium model, Comput. Mater. Sci. 92 (2014) 213–223.

[32] Y. Yu, Y.X. Zhang, Coupling of chemical kinetics and thermodynamics for simulations of leaching of cement paste in ammonium nitrate solution, Cem. Concr. Res. 95 (2017) 95–107.

[33] V.Q. Tran, A. Soive, V. Baroghel-Bouny, Modelisation of chloride reactive transport in concrete including thermodynamic equilibrium, kinetic control and surface complexation, Cem. Concr. Res. 110 (2018) 70–85.

[34] V.Q. Tran, A. Soive, S. Bonnet, A. Khelidj, A numerical model including thermodynamic equilibrium, kinetic control and surface complexation in order to explain cation type effect on chloride binding capability of concrete, Constr. Build. Mater. 191 (2018) 608–618.

[35] B. Guo, Y. Hong, G. Qiao, J. Ou, Z. Li, Thermodynamic modeling of the essential physicochemical interactions between the pore solution and the cement hydrates in chloride-contaminated cement-based materials, J. Colloid Interface Sci. 531 (2018) 56–63.

[36] E. Samson, G. Lemaire, J. Marchand, J.J. Beaudoin, Modeling chemical activity effects in strong ionic solutions, Comput. Mater. Sci. 15 (1999) 285–294.

[37] K. Andersson, B. Allard, M. Bengtsson, B. Magnusson, Chemical composition of cement pore solutions, Cem. Concr. Res. 19 (1998) 327–332.

[38] R. Cherif, A. Hamami, A. Aït-Mokhtar, R. Siddique, Comparison of chemical properties of pore solution of hardened cement pastes containing mineral additions, Adv. Cem. Res. 33 (2021) 331 – 341. https://doi.org/10.1680/jadcr.19.00037.

[39] NT Build 492, Concrete, Mortar and Cement-based Repair Materials: Chloride Migration Coefficient from Non-steady-state Migration Experiments, Nordtest method, 1999.

[40] D. Damidot, F.P. Glasser, 'Thermodynamic investigation of the $CaO-Al_2O_3-CaSO-H_2O$ system at 50°C and 85°C, Cem. Concr. Res. 22 (1992) 1179–1191.

[41] C. Abate, B.E. Scheetz, Aqueous phase equilibria in the system $CaO-Al_2O_3-CaCl_2-H_2O$: The significance and stability of friedels salt, J. Am. Ceram. Soc. 78 (1995) 939–944.

[42] S. Galı□ , C. Ayora, P. Alfonso, E. Tauler, M. Labrador, Kinetics of dolomite–portlandite reaction: Application to portland cement concrete, Cem. Concr. Res. 31 (2001) 933–939.

[43] I. Baur, P. Keller, D. Mavrocordatos, B. Wehrli, C.A. Johnson, Dissolution-precipitation behaviour of ettringite, monosulfate, and calcium silicate hydrate, Cem. Concr. Res. 34 (2004) 341–348.

[44] T. Matschei, B. Lothenbach, F.P. Glasser, Thermodynamic properties of Portland cement hydrates in the system $CaO-Al_2O_3-SiO_2-CaSO_4-CaCO_3-H_2O$, Cem. Concr. Res. 37 (2007) 1379–1410.

[45] B. Lothenbach, T. Matschei, G. Möschner, F.P. Glasser, Thermodynamic modelling of the effect of temperature on the hydration and porosity of Portland cement, Cem. Concr. Res. 38 (2007) 1–18.

[46] M. Balonis, B. Lothenbach, G. Le Saout, F.P. Glasser, Impact of chloride on the mineralogy of hydrated Portland cement systems, Cem. Concr. Res. 40 (2010) 1009–1022.

[47] M. Salgue, A. Sellier, S. Multon, E. Bourdarot, E. Grimal, DEF modelling based on thermodynamic equilibria and ionic transfers for structural analysis, Eur. J. Environ. Civ. Eng. 18 (2014) 377–402.

[48] S. Pradelle, M. Thiéry, V. Baroghel-Bouny, Comparison of existing chloride ingress models within concretes exposed to seawater, Mater. Struct. 49 (2016) 4497–4516.

[49] E.P. Nielsen, D. Herfort, M.R. Geiker, Binding of chloride and alkalis in Portland cement systems, Cem. Concr. Res. 35 (2005) 117–123.

[50] F.P. Glasser, A. Kindness, S.A. Stronach, Stability and solubility relationships in AFm phases: Part I. Chloride, sulfate and hydroxide, Cem. Concr. Res. 29 (1999) 861–866.

[51] C.I. Steefel et al., Reactive transport codes for subsurface environmental simulation, Comput. Geosci. 19 (2015) 445–478: https://doi.org/10.1007/s10596-014-9443-x.

[52] A.C. Lasaga, J.M. Soler, J. Ganor, T. E. Burch, K. L. Nagy, Chemical weathering rate laws and global geochemical cycles, Geochim. Cosmochim. Acta 58 (1994) 2361–2386.

[53] A. Aït-Mokhtar, O. Amiri, O. Poupard, P. Dumargue, A new method for determination of chloride flux in cement-based materials from chronoamperometry, Cem. Concr. Compos. 26 (2004) 339–345.

[54] I. Sánchez, X.R. Nóvoa, G. de Vera, M.A. Climent, Microstructural modifications in Portland cement concrete due to forced ionic migration tests. Study by impedance spectroscopy, Cem. Concr. Res. 38 (2008) 1015–1025.

[55] C. Andrade, J.M. Diez, A. Alamán, C. Alonso, Mathematical modelling of electrochemical chloride extraction from concrete, Cem. Concr. Res. 25 (1995) 727–740.

[56] M. Castellote, C. Andrade, C. Alonso, Phenomenological mass-balance-based model of migration tests in stationary conditions: Application to non-steady-state tests, Cem. Concr. Res. 30 (2000) 1885–1893.

[57] O. Truc, J.P. Ollivier, M. Carcassès, A new way for determining the chloride diffusion coefficient in concrete from steady state migration test, Cem. Concr. Res. 30 (2000) 217–226.

[58] A.A. Hamami, J.M. Loche, A. Aït-Mokhtar, Cement fraction effect on EIS response of chloride migration tests, Adv. Cem. Res. 23 (2011) 233–240.

[59] D.P. Bentz, O.M. Jensen, A.M. Coats, F.P. Glasser, Influence of silica fume on diffusivity in cement-based materials: I. Experimental and computer modeling studies on cement pastes, Cem. Concr. Res. 30 (2000) 953–962.

[60] Y. Guo, T. Zhang, J. Du, C. Wang, J. Wei, Q. Yu, Evaluating the chloride diffusion coefficient of cement mortars based on the tortuosity of pore structurally-designed cement pastes, Microporous Mesoporous Mater. 317 (2021) 111018.

[61] C.A.J. Appelo, L.R. Van Loon, P. Wersin, Multicomponent diffusion of a suite of tracers (HTO, Cl, Br, I, Na, Sr, Cs) in a single sample of Opalinus Clay, Geochim. Cosmochim. Acta 74 (2010) 1201–1219.

[62] Y. Hosokawa, K. Yamada, B. Johannesson, L-O. Nilsson, Development of a multi-species mass transport model for concrete with account to thermodynamic phase equilibriums, Mater. Struct. 44 (2011) 1577–1592.

[63] T. Sanchez, P. Henocq, O. Millet, A. Aït-Mokhtar, Coupling PhreeqC with electro-diffusion tests for an accurate determination of the diffusion properties on cementitious materials, J. Electroanal. Chem. 858 (2020) 113791.

[64] Z. Bajja, W. Dridi, B. Larbi, P. Le Bescop, The validity of the formation factor concept from through-out diffusion tests on Portland cement mortars, Cem. Concr. Compos. 63 (2015) 76–83.

[65] L. Yuan-Hui, S. Gregory, Diffusion of ions in sea water and in deep-sea sediments, Geochim. Cosmochim. Acta 38 (1974) 703–714.

[66] R.S. Barneyback, S. Diamond, Expression and analysis of pore fluids from hardened cement pastes and mortars, Cem. Concr. Res. 11 (1981) 279–285.

[67] E. Conforto, N. Joguet, P. Buisson, J-E. Vendeville, C. Chaigneau, T. Maugard, An optimized methodology to analyze biopolymer capsules by environmental scanning electron microscopy, Mater. Sci. Eng. C. 47 (2015) 357–366.

[68] Q. Huang, C. Wang, Q. Zeng, C. Yang, C. Luo, K. Yang, Deterioration of mortars exposed to sulfate attack under electrical field, Constr. Build. Mater. 117 (2016) 121–128.

[69] S.A. Miller, A. Horvath, P.J.M. Monteiro, Readily implementable techniques can cut annual CO_2 emissions from the production of concrete by over 20%, Environ. Res. Lett. 11 (2016) 074029.

[70] A. Younsi, R. Cherif, A. Trabelsi, A.A. Hamami, R. Belarbi, A. Aït-Mokhtar, Hydration-drying interactions in a high-volume ground granulated blast-furnace slag mortar, Constr. Build. Mater. 279 (2021) 122427.

[71] S.N. Lim, T.H. Wee, Autogenous shrinkage of ground-granulated blast-furnace slag concrete, ACI Mater. J. 95 (2000) 587–593.

[72] O. Amiri, H. Friedmann, A. Aït-Mokhtar, Modelling of chloride-binding isotherm by multi-species approach in cement mortars submitted to migration test, Mag. Concr. Res. 58 (2006) 93–99.

[73] O.R. Ogirigbo, L. Black, Chloride binding and diffusion in slag blends: Influence of slag composition and temperature, Constr. Build. Mater. 149 (2017) 816–825.

[74] P. Refait, A-M. Grolleau, M. Jeannin, E. François, R. Sabot, Corrosion of mild steel at the seawater/sediments interface: Mechanisms and kinetics, Corros. Sci. 130 (2018) 76–84.